Collision Energy Dependence on the Microsolvated S_N2 Reaction of $F^-(H_2O)$ with CH_3Cl: A Full Dimensional Ab Initio Direct Dynamics Study

Hiroto Tachikawa

Division of Molecular Chemistry, Graduate School of Engineering, Hokkaido University, Sapporo 060-8628, Japan

Received: September 13, 2000; In Final Form: November 21, 2000

Collision energy dependence on the microsolvated S_N2 reaction of $F^-(H_2O)$ with CH_3Cl has been investigated by means of direct ab initio dynamics method. A full dimensional ab initio potential energy surface including all degrees of freedom was used in the dynamics calculations; i.e., total energies of the reaction system and gradient of all atoms were calculated at each time step. Three energies, $E_{coll} = 10.0$, 17.7, and 25.0 kcal/mol were chosen as center of mass collision energies between $F^-(H_2O)$ and CH_3Cl. The present dynamics calculations indicated that in all collision energies three reaction channels were open as products. These are expressed by $F^-(H_2O) + CH_3Cl \rightarrow CH_3F + H_2O + Cl^-$ (channel I); $F^-(H_2O) + CH_3Cl \rightarrow CH_3F + Cl^-(H_2O)$ (channel II); and $F^-(H_2O) + CH_3Cl \rightarrow CH_3F{-}H_2O + Cl^-$ (channel III). Channel I is three-body dissociation of each product, whereas Cl^- and CH_3F are solvated by H_2O in channels II and III, respectively. The dynamics calculations also showed that branching rations of channels I:II:III at $E_{coll} = 10.0$, 17.7, and 25.0 kcal/mol are calculated to be 0.55:0.04:0.41, 0.46:0.18:0.36, and 0.35:0.43:0.22, respectively. These results indicate that channels I and III are more favored at lower collision energies and channel II is minor, whereas channel II becomes dominant at higher collision energies. The mechanism of the reaction and the effects of water were discussed on the basis of the present calculations.

1. Introduction

Solvent effects on chemical reaction have been extensively studied from both experimental and theoretical points of view because those play an important role in several reaction systems, especially in biochemical reaction systems. One approach to study molecular processes in solvation systems is to use microsolvation by a finite cluster of molecules. By adding more solvent molecules to the system, one can approach the limiting values of the collective properties observed in the condensed phase. Hence, studying of the microsolvation system gives important information on reactions in both gas and condensed phases.

A lot of work on the nonsolvated bimolecular nucleophilic substitution (S_N2) reactions of type $X^- + CH_3Y$ has been carried out from both experimental and theoretical points of view.[1,2] From an experimental point of view, VanOrder et al. measured the energy distribution of the product ions in a reaction $F^- + CH_3Cl$ using Fourier transform ion cyclotron resonance (FT-ICR) spectroscopy.[3] They showed that almost all available energy is partitioned into the relative translational mode between products. Many ab initio calculations have been carried out for several S_N2 reactions.[2] The energetics and potential energy surfaces (PESs) for both symmetric and asymmetric S_N2 reactions of type $X^- + CH_3Y \rightarrow XCH_3 + Y^-$ were calculated at several levels of theory. Also, the reaction dynamics of the gas-phase S_N2 reactions have been studied by Hase and co-workers using classical trajectory calculation.[4,5] In their calculations, a PES is precalculated by ab initio MO methods, and then it is fitted to analytical functions. They showed that the reaction proceeds via a direct mechanism in which pre- and late-complexes have a very short lifetime at higher collision energy. On the other hand, at lower collision energy, the reaction occurs either via trapping in the $X{-}CH_3Y$ early complex following by non-RRKM dynamics or by direct mechanism which is facilitated C−Y stretch excitation. Later, Hase and co-workers carried out ab initio direct dynamics calculations for the $Cl^- + CH_3Cl$ symmetric S_N2 reaction.[6] They examined the collision of F^- to the backside and frontside of CH_3Cl at high reagent translational energy (100 kcal/mol). The trajectories reacted by a backside attack mechanism, and reaction by frontside attack was not observed.

Recently, we have carried out direct ab initio dynamics calculation on a S_N2 reaction,

$$F^- + CH_3Cl \rightarrow FCH_3 + Cl^-$$

using a full dimensional ab initio PES without analytical fitting.[7,8] In this method, the fitting of potential energy surface to ab initio data is not needed, whereas the ab initio calculation of PES is carried out at each time step during the reaction. We found that the lifetime of the complexes is short enough to proceed via direct mechanism. Also, it was found that the total available energy is divided among the relative translational mode (43%) and the C−F stretching mode (57%) at zero collision energy. The other internal modes of CH_3F remain in the ground state. These features are in good agreement with the previous dynamics studies by Hase and co-workers[5] This means that direct ab initio dynamics calculation, employed in this work, is a useful tool to simulate the S_N2 reaction.

Effects of the solvent molecule on S_N2 reactions have been the focus of extensive experimental[9−17] and theoretical[18−24] work in recent years owing to its central importance in organic chemistry. O'Hair et al. measured the product ions formed by the reaction $F^-(H_2O) + CH_3Cl$ using tandem flowing afterglow selected ion flow tube (SHIFT) technique.[11] They detected two ions Cl^- and $Cl^-(H_2O)$ as products at 300 K. Also, they

10.1021/jp003252v CCC: $20.00
Published on Web 02/02/2001

TABLE 1: Energies of Reactions (in kcal/mol) Calculated Several Levels of Theory.

reaction	HF/3-21+G(d)[a]	HF/6-31G*	MP2/aug-cc-pVTZ[b]	ΔH(expl)
$F^- + CH_3Cl \rightarrow CH_3F + Cl^-$	−34.3	−73.4	−29.6	−31.9
$F^-(H_2O) + CH_3Cl \rightarrow Cl^-(H_2O) + CH_3F$	−29.7	−49.3	−17.4	−24.0
$F^-(H_2O) + CH_3Cl \rightarrow Cl^- + CH_3F + H_2O$	−19.9	−36.9	−2.0	−8.4
$F^-(H_2O) \rightarrow F^- + H_2O$	+14.4	+38.4	+27.6	+23.5
$Cl^- + H_2O \rightarrow Cl^-(H_2O)$	−21.8	−12.4	−15.4	−15.6

[a] Water molecule is expressed by STO-3G basis set. [b] From a reference, Hu, W.-P.; Truhlar, D. G. *J. Am. Chem. Soc*. **1994**, *116*, 7797.

suggested that free Cl^- is a major product, whereas $Cl^-(H_2O)$ is minor. The reaction rate of $F^-(H_2O)$ with CH_3Cl is significantly slower than that of nonsolvated reaction $F^- + CH_3Cl$. Viggiano et al.[10] obtained the similar experimental feature for the reaction $F^-(H_2O) + CH_3Br$: the reaction rate of $F^-(H_2O)$ is about three times slower than that of free F^- ion at 300 K. In their experiment, the product-solvated ion $Br^-(H_2O)$ is estimated to be 0−20% of total ions ($Br^-(H_2O)$ and Br^-). This means that the exchange reaction of H_2O from F^- to Br^- does not occur efficiently in the microsolvated reactions.

From the theoretical point of view, Truhlar and co-workers investigated microsolvated S_N2 reactions of type $X^-(H_2O) + CH_3Y$ (X = F and Cl) by means of ab initio MO calculations.[19−21] In the case of the symmetric S_N2 reaction $Cl^-(H_2O) + CH_3Cl$, it was determined that the transition state (TS) has a C_{2v} symmetry. However, TS was not found in asymmetric reaction $F^-(H_2O) + CH_3Cl$. This means that static ab initio MO calculation may be impossible for such reaction systems.

In a previous paper, we studied the reaction of $F^-(H_2O)$ with CH_3Cl by means of direct ab initio dynamics method.[24] We found that the reaction is composed of three channels as reactive collisions. These are expressed by

$$F^-(H_2O) + CH_3Cl \rightarrow CH_3F + H_2O + Cl^- \quad \text{(channel I)}$$

$$F^-(H_2O) + CH_3Cl \rightarrow CH_3F + Cl^-(H_2O) \quad \text{(channel II)}$$

$$F^-(H_2O) + CH_3Cl \rightarrow CH_3F{-}H_2O + Cl^- \quad \text{(channel III)}$$

The first channel is the three-body dissociation of each product (channel I), whereas Cl^- and CH_3F are solvated by H_2O in channels II and III, respectively. In channels I and III the product ion is Cl^-, whereas the product in channel II is $Cl^-(H_2O)$. Thus, direct ab initio dynamics calculations gave important information on the microsolvated S_N2 reaction dynamics. However, the results presented in the previous paper were obtained for only one collision energy of 4.42 kcal/mol. Therefore, detailed dynamics were not clearly understood. In particular, information on the branching ratios for the product channels was not obtained yet.

In this paper, we investigated the microsolvated S_N2 reaction of $F^-(H_2O)$ with CH_3Cl at the wide collision energy range (i.e., E_{coll} = 10.0, 17.7, and 25.0 kcal/mol) by means of ab initio dynamics calculation. Our interest focuses mainly on collision energy dependence of the branching ratios of the reaction channels. In addition, the effect of the H_2O molecule on the reaction dynamics is examined in order to elucidate role of water molecules on the reaction dynamics in a microsolvated S_N2 reaction.

2. Computational Methods

The present reaction system, $F^-(H_2O) + CH_3Cl$, has a large number of degrees of freedom (3N − 6 = 21), so that it is quite difficult to fit ab initio surface to analytical functions of interatomic potential. Hence, direct ab initio dynamics calculation[25] is the best way to treat the reaction dynamics for the present reaction system. In this work, we used direct ab initio dynamics calculation using the full dimensional potential energy surface.

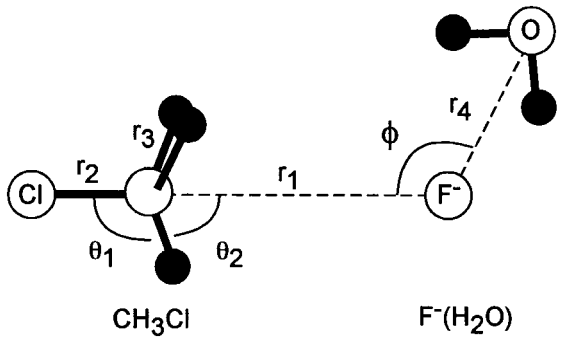

Figure 1. Geometrical parameters for the reaction system $F^-(H_2O) + CH_3Cl$.

In previous papers,[7,8] we showed that HF/3-21+G(d) calculations give a reasonable PES and dynamics features for the reaction $F^- + CH_3Cl \rightarrow FCH_3 + Cl^-$ and also for the microsolvated S_N2 reaction $F^-(H_2O) + CH_3Cl$.[24] Therefore, we used the 3-21+G(d) basis set in the direct ab initio dynamics calculations. The water molecule is expressed by the STO-3G basis set.

The relative energies calculated at the several levels of theory and corresponding experimental values are given in Table 1. As shown in this table, HF/3-21+G(d) calculations would give reasonable energies for the present system.

The optimized geometries of CH_3Cl and $F^-(H_2O)$ were chosen as an initial structure. At the start of the trajectory calculation, atomic velocities of CH_3Cl and $F^-(H_2O)$ were adjusted to give a temperature of 10 K as classical vibrational distribution. Temperature of the reaction system is defined by

$$T = \frac{1}{3kN}\langle m_i v_i^2 \rangle$$

where N is the number of atoms, v_i and m_i are velocity and mass of the ith atom, and k is Boltzmann's constant. Figure 1 shows the structure and geometrical parameters of the reaction system. The angle ϕ is defined by ∠C−F−O. Prior to the effective trajectory calculations, we tested 50 preliminary trajectories from the geometrical conformations selected randomly in the range ϕ = 0−180°. The results indicated that the trajectories with angles smaller than ϕ = 90° became nonreactive. Therefore, we choose the angles in the range ϕ = 70−180° for the initial conformations in the effective dynamics calculation. Next, the angle ϕ is divided by each 10 degree within the range ϕ = 70−180°. Five initial configurations were randomly selected in each divided angle. The initial separations (i.e., r_2 distance) were also generated within r_2 = 6.5−8.0 Å. A total of 55 geometrical configurations were randomly selected, and 55 trajectories were run for each collision energy (E_{coll}).

We chose three collision energies: $E_{coll} = 10.0$, 17.7, and 25.0 kcal/mol. The equations of motion for n atoms in the reaction system are given by

$$\frac{dQ_j}{dt} = \frac{\partial H}{\partial P_j}$$

$$\frac{\partial P_j}{\partial t} = -\frac{\partial H}{\partial Q_j} = -\frac{\partial U}{\partial Q_j}$$

where $j = 1-3N$, H is the classical Hamiltonian, Q_j is the Cartesian coordinate of the jth mode, and P_j is the conjugated momentum. These equations were solved numerically by the standard fourth-order Runge−Kutta and sixth-order Adams−Moulton combined algorithm. No symmetry restriction was applied to the calculation of the gradients. The time step size was chosen by 0.10 fs, and a total of 10 000 steps was calculated for each dynamics calculation. The drift of the total energy is confirmed to be less than 0.1% throughout at all steps in the trajectory. The momentum of the center of mass and the angular momentum are assumed to be zero. Static ab initio MO calculations were carried out using the Gaussian 94 program[26] in order to obtain more accurate energetics.

3. Results

The dynamics calculations at all collision energies showed that three reaction channels were concerned with the reaction as the products. These are expressed by

$$F^-(H_2O) + CH_3Cl \rightarrow CH_3F + H_2O + Cl^- \quad \text{(channel I)}$$

$$F^-(H_2O) + CH_3Cl \rightarrow CH_3F + Cl^-(H_2O) \quad \text{(channel II)}$$

$$F^-(H_2O) + CH_3Cl \rightarrow CH_3F{-}H_2O + Cl^- \quad \text{(channel III)}$$

Channel I is a three-body dissociation channel where all products ($CH_3F + H_2O + Cl^-$) are separate from each other. The H_2O molecule is dissociated from F^- after Walden inversion, and it is mainly scattered in the direction opposite to Cl^-. In channel II, the product Cl^- is solvated by a water molecule. The H_2O molecule moves over the methyl group in the course of Walden inversion, and the H_2O molecule pursues the dissociating Cl^-. Thus, Cl^- is solvated by H_2O in channel II. The product CH_3F is solvated by H_2O in channel III. H_2O is still connecting to the F atom of CH_3F after Walden inversion. These feature are the same as that of our previous study using $E_{coll} = 4.42$ kcal/mol.[16] In this section, we explain the result for channel II in order to elucidate the reaction dynamics in detail, since details of channels I and III are already described in the previous paper.[16]

A. Sample Trajectory for Channel II. *Snapshots.* Snapshots of the geometrical configuration of the reaction system are given in Figure 2. This is a typical trajectory for channel II. At time zero, $F^-(H_2O)$ is located at 8.399 Å from CH_3Cl as the C−F distance (r_1), and the angle ϕ is 116.2°. The center of mass collision energy is 25 kcal/mol. At time 0.21 ps, $F^-(H_2O)$ approaches CH_3Cl at $r_1 = 2.714$ Å, which is enough to interact as ion−dipole complex. The stabilization energy of the complex at this point is 13 kcal/mol relative to the initial separation. The C−Cl distance of CH_3Cl is slightly elongated by the complex formation, but the change of the distance is small (0.07 Å). In the vicinity of TS (time = 0.235 ps), F^- collides with the carbon atom of CH_3Cl, and the C−Cl bond of CH_3Cl is elongated to

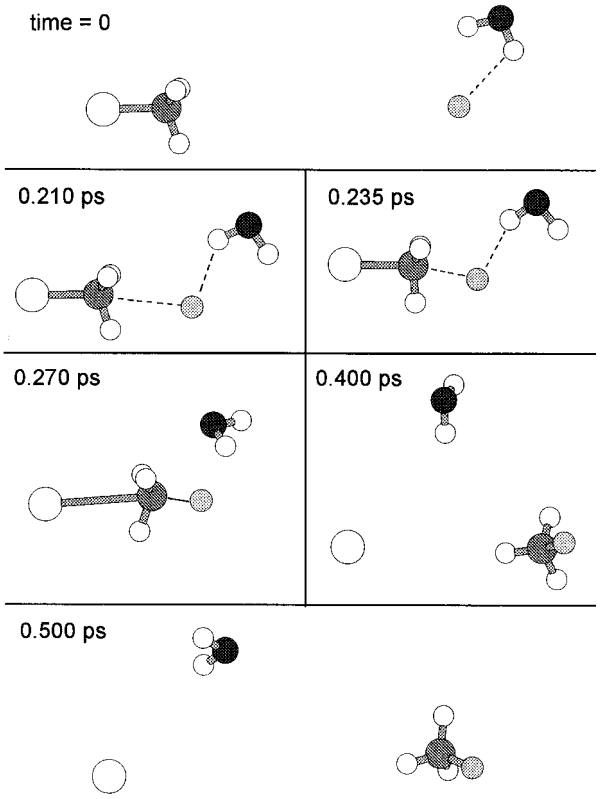

Figure 2. Snapshots of the conformations for the sample trajectory (channel II) illustrated as a function of reaction time. Initial parameters are the distances $r_1 = 8.399$, $r_2 = 1.806$, $r_3 = 1.076$ Å, and $r_4 = 2.828$, and angles $\theta_1 = 108.2°$ and $\phi = 116.2°$. Center-of-mass collision energy (E_{coll}) is 25.0 kcal/mol. The 3-21+G* and STO-3G basis sets were used for $CH_3Cl + F^-$ and H_2O, respectively.

be 1.958 Å (the corresponding distance is 1.806 Å, and angle θ_1 is 108.2° at time zero), and the moiety of CH_3 is significantly close to planar ($\theta_1 = 94.2°$). The position of H_2O relative to the C−F axis (defined by ϕ) is almost constant ($\phi = 116.2-116.7°$) during the approach. After passing TS, the angle of CH_3 (θ_1) is largely changed to 66.3°, meaning that a Walden inversion occurs. At time 0.270 ps, the C−Cl and C−F bond distances are calculated to be 3.053 and 1.420 Å, respectively. This means that the bond-breaking and forming occurs in this region. The angle ϕ is 93.0° at 0.27 ps, meaning that the H_2O molecule begins to exceed over the methyl group. At time 0.400 ps, the H_2O molecule exceeded over the methyl group ($\phi = 60.0°$) and pursues the Cl^- ion. The H_2O and Cl^- are located at the distances 5.516 and 7.702 Å far from CH_3F, respectively. Thus, it is clearly seen in Figure 3 (0.50 ps) that the H_2O pursues the leaving Cl^- ion after the Walden inversion.

Potential Energy of the Reaction System. To elucidate the reaction dynamics of $F^-(H_2O)$ with CH_3Cl, time dependence of the potential energy, intra- and intermolecular distances and angles are plotted in Figure 3. This trajectory corresponds to that given in Figure 2. The potential energy of the reaction system (PE) plotted as a function of reaction time is given in Figure 3A. Parts B and C of Figure 3 indicate the bond distances (r_1, r_2, and r_4) and angles (θ_1 and θ_2), respectively.

At time zero, $F^-(H_2O)$ is located at $r_1 = 8.399$ Å from CH_3-Cl, while the distance between H_2O and F^- is 3.076 Å as the O−F distance ($= r_4$). After starting the reaction, PE decreases gradually as the reaction time is increased, and it reaches −13.0 kcal/mol at time 0.210 ps. During this process, the distance r_1 decreases linearly as a function of reaction time. This means that the approaching of $F^-(H_2O)$ to CH_3Cl causes an energy

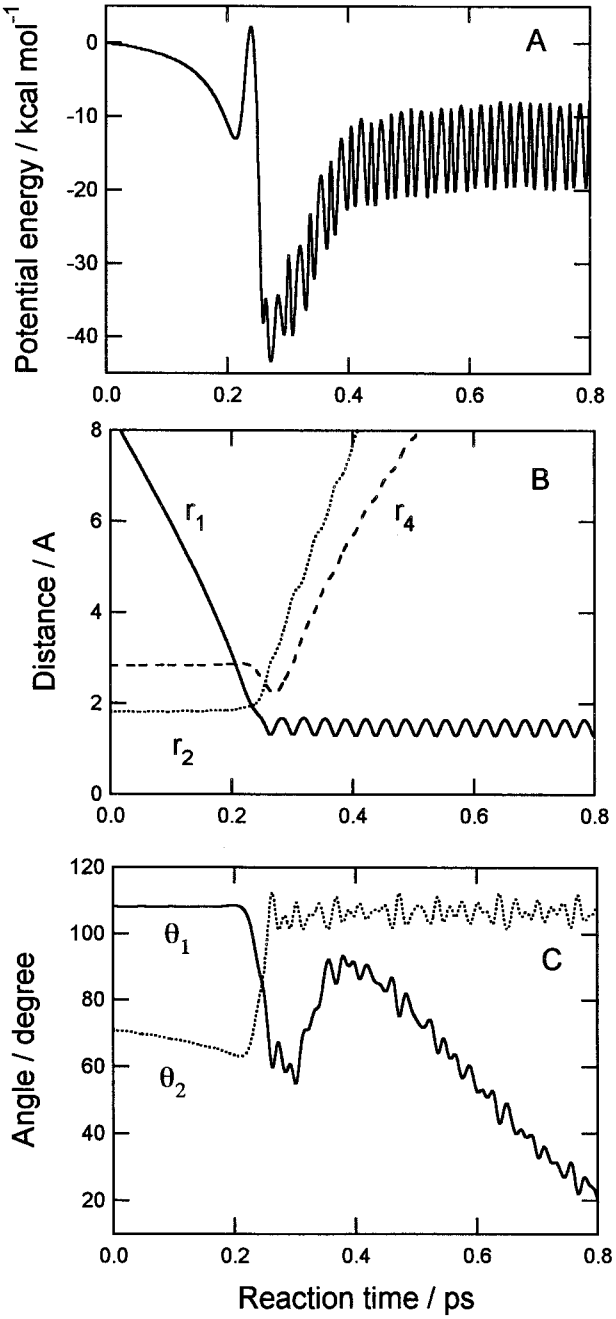

Figure 3. Sample trajectory for channel II. (A) Potential energy of the system, (B) interatomic distances, and (C) angles vs reaction time. Initial condition of the trajectory calculation is the same as that in Figure 2.

lowering due to the attractive ion−dipole interaction. At 0.210 ps, PE reaches a minimum corresponding to precomplex expressed by $(H_2O)F^-—CH_3Cl$. The lifetime of the complex is very short (τ < 30 fs), and the trajectory rapidly reaches the transition state (TS). In the case of this trajectory, the dynamical barrier height at the TS is calculated by 2.2 kcal/mol relative to the initial separation. After the TS, PE decreases suddenly to −43.4 kcal/mol at 0.27 ps, and then it increases gradually to −19.8 kcal/mol at 0.40 ps. The basin of PE with stabilization energy of 43.4 kcal/mol is caused by the formation of the late complex $Cl^-—CH_3F—H_2O$. After that, PE vibrates strongly with amplitude of 11.9 kcal/mol.

The structures of the reaction system are largely changed in the course of reaction. After starting the trajectory calculation, the distance r_1 decreases gradually as reaction time is increased.

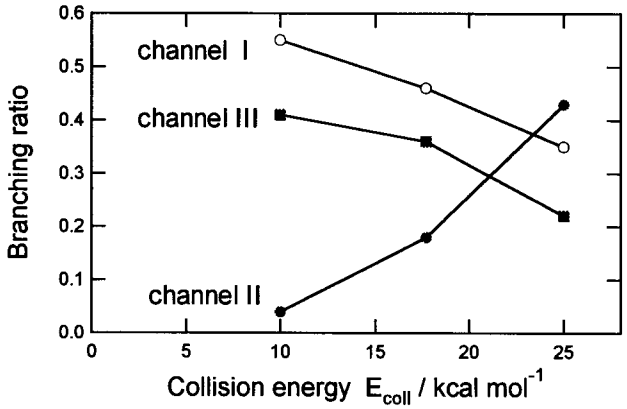

Figure 4. Branching ratios for channels I, II, and III plotted as a function of collision energy.

And then, the precomplex expressed by $(H_2O)F^-—CH_3Cl$ is formed at time 0.210 ps. The structure of CH_3Cl (r_2 = 1.806 Å) is slightly changed before and after the complex formation: the C−F distance is elongated (r_2 = 1.875 vs 1.806 Å), and the umbrella of CH_3Cl is slightly changed (θ_2 is varied from 70.9 to 62.0° by the complex formation). This structural change is due to the fact that interaction between $F^-(H_2O)$ and CH_3Cl is mainly composed of ion−dipole. After passing TS, the structures are drastically changed: the angles θ_1 and θ_2 are varied in the range θ_1 = 55.1−108.5° and θ_2 = 62.0−112.4°, respectively, meaning that a Walden inversion occurs in this region. The C−H bond of CH_3 methyl group (r_3) is almost constant during the reaction, indicating that the excess energy is not dedicated efficiently into the C−H stretching mode. The distance r_1 vibrates in the range 1.282−1.645 Å, indicating that the bond C−F is newly formed, and the stretching mode of C−F is slightly excited after TS. The Cl^- ion leaves from CH_3F, as clearly seen in Figure 3B (r_2). Time dependence of distance r_4 means the H_2O molecule also leaves from CH_3F and it pursues the leaving Cl^- ion. Therefore, this channel corresponds to channel II: namely, the products are CH_3F and $Cl^-(H_2O)$.

B. Collision Energy Dependence of the Product Branching Ratios. A total of 165 trajectories were run for three center-of-mass collision energies (E_{coll} = 10.0, 17.7, and 25.0 kcal/mol). The branching ratios for each reaction channel are plotted in Figure 4 as a function of center-of-mass collision energy E_{coll}. At lower collision energy (E_{coll} = 10.0 kcal/mol), the branching ratio I:II:III is calculated to be 0.55:0.04:0.41, indicating that the main channel is three-body dissociation (channel I). Also, the ratio of channel III is relatively large. On the other hand, it is clearly seen that channel II is minor. At E_{coll} = 17.7 kcal/mol, the branching ratio (I:II:III) becomes 0.46:0.18:0.36. The ratio of channel II is about 5 times larger than that at E_{coll} = 10.0 kcal/mol. However, channel I is still the main channel. The branching ratio at E_{coll} = 25.0 kcal/mol is calculated to be 0.35:0.43:0.22, meaning that channel II becomes main channel. The ratio of channel II is about 10 times larger than that at E_{coll} = 10.0 kcal/mol. Thus, the product branching ratio is significantly affected by the center of mass collision energy. In particular, the present calculations predict that channel II becomes the main channel if the reaction may occur at higher collision energies, larger than 20−25 kcal/mol.

C. Dominant Factor on the Reaction Channels. In the previous section, we showed that three reaction channels proceed competitively with each other. Here, let us consider the question "What is dominant factor in the reaction channels?". For such purpose, we analyze the mutual relation between the initial position of H_2O and its final product channel. The position of

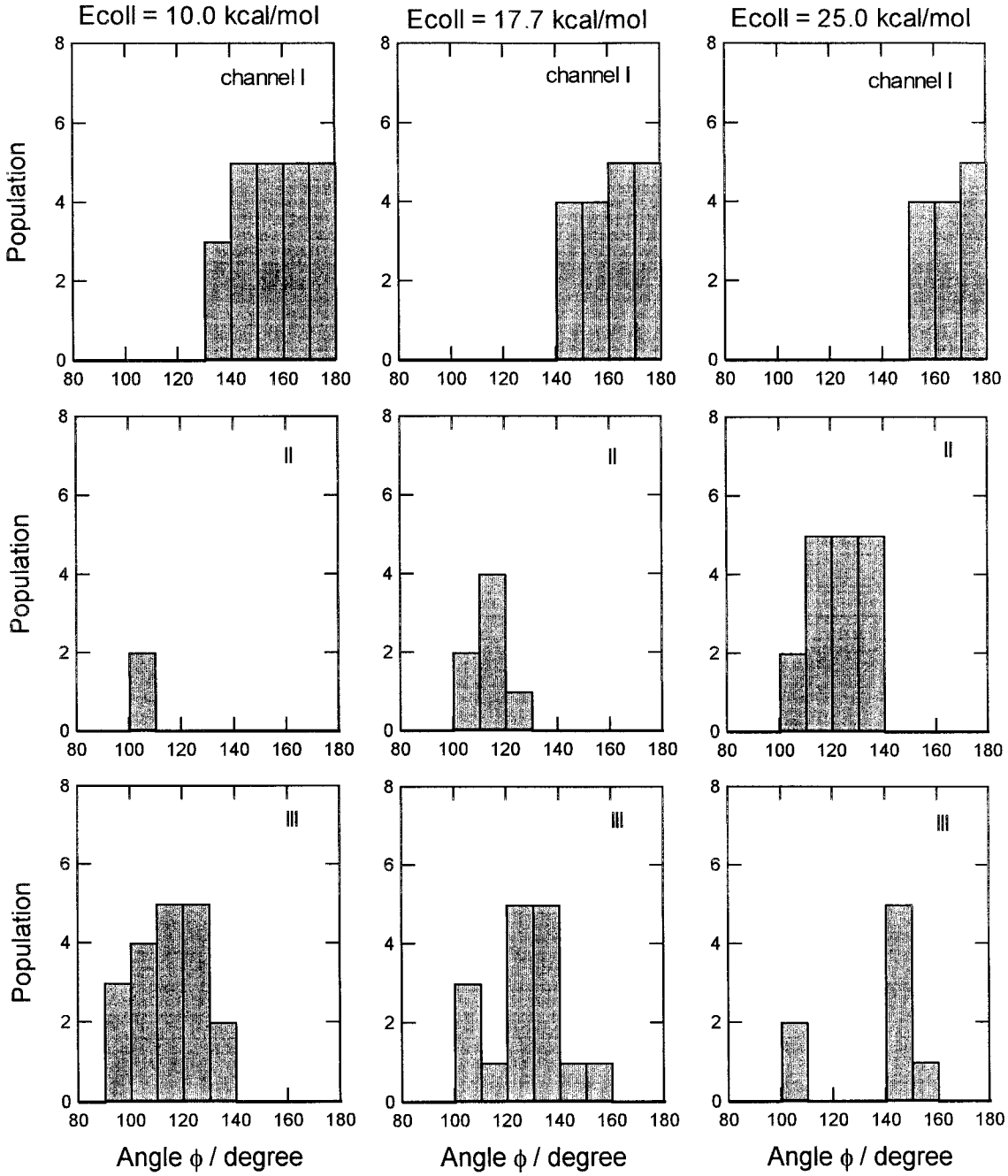

Figure 5. Relative populations of the product channels (I, II, and III) plotted as a function of angle ϕ. Left, middle, and right panels indicate the populations obtained for $E_{coll} = 10.0$, 17.7, and 25.0 kcal/mol, respectively. The products for channels I, II, and III are [$CH_3F + Cl^- + H_2O$], [$CH_3F + Cl^-(H_2O)$], and [CH_3F- -$H_2O + Cl^-$], respectively.

H_2O relative to the C−F axis is defined by the angle ϕ. For example, in the case of $\phi = 180°$, H_2O is located at the position opposite to CH_3Cl: namely, F^- is located in middle between CH_3Cl and H_2O. On the other hand, in the case of $\phi = 90°$, H_2O is located above F^-. In the latter case, H_2O collides simultaneously the methyl group of CH_3Cl when F^- collides with the carbon atom of CH_3Cl, whereas only F^- ion collides CH_3Cl in the former case.

The population of each product channel, plotted as a function of angle ϕ, is given in Figure 5. As clearly seen in this Figure, the reaction channels are affected significantly by the position of H_2O (angle ϕ). Three panels in left side of Figure 5 indicate populations of channels I (upper), II(middle), and III (lower) produced at $E_{coll} = 10.0$ kcal/mol. Collision with $\phi = 130-180°$ leads to three-body dissociation products ($CH_3F + Cl^- + H_2O$, i.e., channel I). This channel occurs from the wide region ($\phi \approx 140-180°$), and the population is widely and highly distributed. On the other hand, the products $CH_3F + Cl^-(H_2O)$ in channel II are formed from a very narrow region ($\phi = 100-110°$), and the population of channel II is smaller than those of the other channels. The population of channel III is distributed in the range $\phi = 90-140°$. The collisions with angles smaller than 90° lead to nonreactive channel because the H_2O molecule prevents access of F^- to CH_3Cl.

At $E_{coll} = 17.7$ kcal/mol, distribution of channel II is spread in the range $\phi = 100-130°$. On the other hand, distribution of channel I becomes slightly narrow and is shifted to larger angle region ($\phi = 140-180°$). At higher collision energy ($E_{coll} = 25.0$ kcal/mol), the distribution of channel II is wide, whereas that of channel I becomes more narrow ($\phi = 150-180°$). The

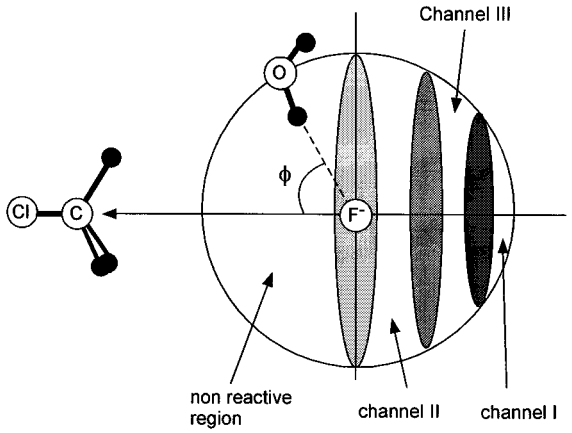

Figure 6. The reaction model for the microsolvated S_N2 reaction, $F^-(H_2O) + CH_3Cl$. Spherical surface means the position of H_2O around F^- at the initial separation. The position of H_2O is defined by the angle O−F−C (= ϕ).

distribution of channel III is separated by two parts: these are distributed in the range 100−110° and 140−160°. These results strongly indicate that the reaction channels are dominant by the relative position of H_2O.

4. Discussion

A. The Reaction Model. The present calculations showed that the reaction channels are strongly affected by the relative position of H_2O at the initial separation. Since the collision of $F^-(H_2O)$ with CH_3Cl occurs randomly in gas phase, the position of H_2O in the initial separation is expressed by a spherical surface around the F^- ion as shown in Figure 6. Figure 6 also shows the reaction model proposed on the basis of the present calculations. Each trajectory starts from a point somewhere on the spherical surface. If H_2O is located in the region with angles smaller than $\phi = 90°$ (i.e., the left half of the spherical surface), all trajectories from the region lead to the nonreactive channel. The right half of the spherical surface becomes the main reactive channels (I, II, and III). This means that the reactive collision of $F^- + CH_3Cl$ is deduced to at least 1/2 in the case of the microsolvated S_N2 reaction system $F^-(H_2O) + CH_3Cl$.

As shown in section 3C, channel I occurs mainly at angles larger than ϕ close to 180°. This is due to the fact that the collision energy is efficiently transferred into the CH_3F-H_2O intermolecular stretching mode after the collision of $F^-(H_2O)$ to CH_3Cl, so that H_2O can leave from CH_3F. The product channel becomes a three-body dissociation. Channel II occurs at very narrow angles ($\phi = 100-110°$) in a low collision energy region because H_2O should exceed the methyl group of CH_3F after a Walden inversion. The activation process needs in channel II. Channel III occurs at the middle of the angles ($\phi = 100-150°$), and it occurs at wide region even at the low collision energy. This is due to the fact that the solvation of CH_3F by H_2O proceeds easily before and after Walden inversion. Thus, it is shown that the position of H_2O affects strongly the microsolvated S_N2 reaction dynamics.

As a traditional picture in microsolvated S_N2 reactions, it has been confirmed that the barrier height of transition state increases with increasing solvent molecules.[20−23] This solvent effect decreases strongly the reaction rate. The present calculations suggest that, in addition to the solvent effect on the barrier height, the position of H_2O surrounding the reagent ions affects the reaction probability as a dynamical effect.

B. Branching Ratios. Next, we should consider the question "Why is the branching ratio of channel II smaller than the other channels at lower collision energy?". The heat of reaction for channel II is larger than those of the other channels ($-\Delta H$ for channels I, II, and III are 11, 24, and 16 kcal/mol, respectively). However, the ratio of channel II is significantly small at low collision energy. This answer is already suggested in section 4A. In the case of channel II, the H_2O molecule should exceed the methyl group of CH_3Cl, and then it should pursue Cl^- after the Walden inversion. This process needs a slight activation energy, and this energy should be given by translational energy of H_2O. The translational energy of H_2O is too small to exceed the methyl group at lower collision energy, so that the trajectory leads to three-body dissociation or solvation of CH_3F. Hence, the H_2O molecule located only at a limited angle (ϕ) can proceed over CH_3Cl, while the branching ratio of channel II is significantly small at low collision energy. At higher collision energies, H_2O, which is located at wide angles ($\phi = 100-140°$), can proceed over the CH_3 group, and the H_2O molecule can solvate Cl^- after the Walden inversion. This is the origin of the strong collision energy dependence of the branching ratio.

C. Comparison with the Experiments. The present calculations showed that the trajectories started from left half ($\phi < 90°$) become the nonreactive channel. This means that the reaction probability of $F^-(H_2O)$ deduces at least 1/2 compared with no solvent reaction system ($F^- + CH_3Cl$). In addition, some trajectories from the right half of spherical surface become nonreactive collisions. Furthermore, preliminary calculations for the trajectories with larger impact parameters showed that reactive trajectories decreases suddenly with increasing impact parameter compared with nonsolvated reaction. This is due to the steric effect of H_2O. Thus, the H_2O molecule reduces significantly the reaction probability.

O'Hair et al. measured reaction rates for $F^-(H_2O) + CH_3Cl$ and $F^- + CH_3Cl$ using tandem flowing afterglow selected ion flow tube technique. They showed that ratio of the reaction rates $k[F^-(H_2O)]/k[F^-]$ is measured by 1/95 at 300 K. A similar feature was obtained for the reaction of $F^-(H_2O)$ with CH_3Br by Viggiano et al. They measured the ratio of the reaction rates to be $k[F^-(H_2O)]/k[F^-] = 1/3$. Thus, their experimental finding is explained reasonably in terms of the present model.

D. Concluding Remarks. We have introduced several approximations to calculate the potential energy surface and to treat the reaction dynamics. First, we assumed HF/3-21+G(d) multidimensional potential energy surface in the trajectory calculations throughout. As shown in previous papers, the shape of PES for the $F^- + CH_3Cl$ reaction system calculated at the HF/3-21+G(d) level of theory is in good agreement with that of QCISD/6-311G(d,p) level. Therefore, it is enough to discuss qualitatively the reaction dynamics for the $F^-(H_2O) + CH_3Cl$ reaction system. However, a more accurate wave function may provide deeper insight in the dynamics. Second, we calculated 55 trajectories for each collision energy ($E_{coll} = 10.0$, 17.7, and 25.0 kcal/mol). In addition, we considered trajectories with near zero-impact parameters. The number of trajectories may be enough to discuss the qualitative feature of the dynamics. However, a large number of trajectories with larger impact parameters are needed in order to obtain a more accurate reaction rate. Despite the several assumptions introduced here, the results enable us to obtain valuable information on the mechanism of the microsolvated S_N2 reaction.

Acknowledgment. The author is indebted to the Computer Center at the Institute for Molecular Science (IMS) for the use of the computing facilities. I also acknowledge partial support

from a Grant-in-Aid from the Ministry of Education, Science, Sports and Culture of Japan.

References and Notes

(1) For a selection of experimental works on gas-phase S_N2 reaction, see: (a) Olmstead, W. N.; Brauman, J. I. *J. Am. Chem. Soc.* **1977**, *99*, 44219. (b) Su, T.; Morris, R. A.; Viggiano, A. A.; Paulson, J. F. *J. Phys. Chem.* **1990**, *94*, 8426. (c) Viggiano, A. A.; Paschkewitz, J. S.; Morris, R. A.; Paulson, J. F.; Gonzalez-Lafont, A.; Truhlar, D. G. *J. Am. Chem. Soc.* **1991**, *113*, 9404. (d) DePuy, C. H.; Gronert, S.; Mullin, A.; Bierbaum, V. M. *J. Am. Chem. Soc.* **1990**, *112*, 2, 8650. (e) Gronert, S.; DePuy, C. H.; Bierbaum, V. M. *J. Am. Chem. Soc.* **1991**, *113*, 4009. (f) Graul, S. T.; Bowers, M. T. *J. Am. Chem. Soc.* **1991**, *113*, 9696. (g) Graul, S. T.; Bowers, M. T. *J. Am. Chem. Soc.* **1994**, *116*, 3875. (h) Van Orden, S. L.; Pope, R. M.; Buckner, S. W. *Org. Mass Spectrom.* **1991**, *26*, 1003. (i) Cyr, D. M.; Posey, L. A.; Bishea, G. A.; Han, C.-C.; Johnson, M. A. *J. Am. Chem. Soc.* **1991**, *113*, 9697. (j) Cyr, D. M.; Bishea, G. A.; Scarton, M. G.; Johnson, M. A. *J. Chem. Phys.* **1992**, *97*, 5911. (k) Giles, K.; Grimsrud, E. P. *J. Phys. Chem.* **1992**, *96*, 6680. Knighton, W. B.; Boghar, J. A.; O'Connor, P. M.; Grimsrud, E. P. *J. Am. Chem. Soc.* **1993**, *115*, 12079. (l) Sahlstrom, K. E.; Knighton, W. B.; Grimsrud, E. P. *J. Phys. Chem. A* **1997**, *101*, 1501. (m) Viggiano, A. A.; Morris, R. A.; Paschkewitz, J. S.; Paulson, J. F. *J. Am. Chem. Soc.* **1992**, *114*, 10477. (n) Wladkowski, B. D.; Lim, K. F.; Allen, W. D.; Brauman, J. I. *J. Am. Chem. Soc.* **1992**, *114*, 9136. (o) Viggiano, A. A.; Morris, R. A.; Su, T.; Wladkowski, B. D.; Craig, S. L.; Zhong, M.; Brauman, J. I. *J. Am. Chem. Soc.* **1994**, *116*, 2213. (p) Craig, S. L.; Brauman, J. I. *Science* **1997**, *276*, 1536. (q) Viggiano, A. A.; Morris, R. A. *J. Phys. Chem.* **1994**, *98*, 3740. (r) Li, C.; Ross, P.; Szulejko, J. E.; McMahon, T. B. *J. Am. Chem. Soc.* **1996**, *118*, 9360. (s) Craig, S. L.; Brauman, J. I. *J. Phys. Chem. A* **1997**, *101*, 4745. (t) DeTuri, V. F.; Hintz, P. A.; Ervin, K. M. *J. Phys. Chem. A* **1997**, *101*, 5969. (u) Seeley, J. V.; Morris, R. A.; Viggiano, A. A.; Wang, H.; Hase, W. L. *J. Am. Chem. Soc.* **1997**, *119*, 577. (v) Le Garrec, J.-L.; Rowe, B. R.; Queffelec, J. L.; Mitchell, J. B. A.; Clary, D. C., *J. Chem. Phys.* **1997**, *107*, 1021. (w) Chabinyc, M. L.; Craig, S. L.; Regan, C. K.; Brauman, J. I. *Science* **1998**, *279*, 1882.

(2) For a selection of theoretical studies of S_N2 reactions, see: (a) Ryaboy, V. M. In *Advances in Classical Trajectory Methods*; Hase, W. L., Ed.; JAI Press: Greenwich, CT, 1994; Vol. 2, pp 115−145. (b) Vande Linde, S. R.; Hase, W. L. *J. Phys. Chem.* **1990**, *94*, 2778. (c) Tucker, S. C.; Truhlar, D. G. *J. Am. Chem. Soc.* **1990**, *112*, 3338. (d) Billing, G. D. *Chem. Phys.* **1992**, *159*, 109. (e) Wladkowski, B. D.; Allen, W. D.; Brauman, J. I. *J. Phys. Chem.* **1994**, *98*, 13532. (f) Wang, H.; Zhu, L.; Hase, W. L. *J. Phys. Chem.* **1994**, *98*, 1608. (g) Wang, H.; Hase, W. L. *J. Am. Chem. Soc.* **1995**, *117*, 9347. (h) Hu, W.-P.; Truhlar, D. G. *J. Am. Chem. Soc.* **1995**, *117*, 10726. (i) Glukhovtsev, M. N.; Pross, A.; Radom, L. *J. Am. Chem. Soc.* **1995**, *117*, 2024. (j) Glukhovtsev, M. N.; Pross, A.; Radom, L. *J. Am. Chem. Soc.* **1996**, *118*, 6273. (k) Wang, H.; Hase, W. L. *Chem. Phys.* **1996**, *212*, 247. (l) Clary, D. C.; Palma, J. *J. Chem. Phys.* **1996**, *106*, 575. (m) Wang, H.; Goldfield, E. M.; Hase, W. L. *J. Chem. Soc., Faraday Trans.* **1997**, *93*, 737. (n) Botschwina, P.; Horn, M.; Seeger, S.; Oswald, R. *Ber. Bunsen-Ges. Phys. Chem.* **1997**, *101*, 387. (o) Baer, T.; Hase, W. L. In *Unimolecular Reaction Dynamics-Theory and Experiments*; Oxford: New York, 1996.

(3) VanOrden, S. L.; Pope, R. M.; Buckner, S. W. *Org. Mass Spectrom.* **1991**, *26*, 1003.

(4) (a) Wang, H.; Hase, W. L. *J. Am. Chem. Soc.* **1997**, *199*, 3093. (b) Craig, S. L.; Brauman, J. I. *J. Phys. Chem. A* **1997**, *101*, 4745.

(5) Trajectory studies for the S_N2 reaction (a) Vande Linde, S. R.; Hase, W. L. *J. Phys. Chem.* **1990**, *94*, 6148. (b) Vande Linde, S. R.; Hase, W. L. *J. Chem. Phys.* **1990**, *93*, 7962. (c) Peslherbe, G. H.; Wang, H.; Hase, W. L. *J. Chem. Phys.* **1995**, *102*, 5626. (d) Cho, Y. J.; Vande Linde, S. R.; Zhu, L.; Hase, W. L. *J. Chem. Phys.* **1992**, *96*, 8275. (e) Hase, W. L.; Cho, Y. J. *J. Chem. Phys.* **1993**, *98*, 8626. (f) Wang, H.; Peslherbe, G. H.; Hase, W. L. *J. Am. Chem. Soc.* **1994**, *116*, 9644. (g) Peslherbe, G. H.; Wang, H.; Hase, W. L. *J. Am. Chem. Soc.* **1996**, *118*, 2257. (h) Hase, W. L. *Science* **1994**, *266*, 998. (i) Wang, H. Hase, W. L. *Int. J. Mass Spectrom. Ion Processes* **1997**, *167/168*, 573, 22.

(6) Li, G.; Hase, W. L. *J. Am. Chem. Soc.* **1999**, *121*, 7124.

(7) Tachikawa, H.; Igarashi, M. *Chem. Phys. Lett.* **1999**, *303*, 81.

(8) Igarashi, M.; Tachikawa, H. *Int. Mass Spectrom.* **1998**, *181*, 151.

(9) Seeley, J. V.; Morris, R. A.; Viggiano, A. A.; Wang, H.; Hase, W. L. *J. Am. Chem. Soc.* **1997**, *119*, 577.

(10) Viggiano, A. A.; Arnold, S. T.; Morris, R. A.; Ahrens, A. F.; Hierl, P. M. *J. Phys. Chem*. **1996**, *100*, 14397.

(11) O'Hair, R. A.; Davico, G. E.; Hacaloglu, J.; Dang, T. T.; DePuy, C. H.; Bierbaum, V. M. *J. Am. Chem. Soc.* **1994**, *116*, 3609.

(12) Hierl, P. M.; Ahrens, A. F.; Henchman, M.; Viggiano, A. A., Paulson, J. F. *J. Am. Chem. Soc.* **1986**, *108*, 3142.

(13) Henchman, M.; Hierl, P. M.; Paulson, J. F. *J. Am. Chem. Soc.* **1985**, *107*, 2812.

(14) Bohme, D. K.; Raksit, A. B. *Can. J. Chem.* **1985**, *63*, 3007.

(15) Henchman, M.; Paulson, J. F.; Hierl, P. M. *J. Am. Chem. Soc.* **1983**, *105*, 5509.

(16) Bohme, D. K.; Raksit A. B. *J. Am. Chem. Soc.* **1984**, *106*, 3447.

(17) Borme, D. K.; Mackay G. I. *J. Am. Chem. Soc.* **1981**, *103*, 978.

(18) Okuno, Y. *J. Chem. Phys.* **1996**, *205*, 5817.

(19) Zhao, X. G.; Lu, D.-H, Liu, Y.-P.; Lynch, G. C.; Truhlar, D. G. *J. Chem. Phys.* **1992**, *97*, 6369.

(20) Zhao, X. G.; Tucker, S. C.; Truhlar, D. G. *J. Am. Chem. Soc.* **1991**, *113*, 826.

(21) Tucker, S. C.; Truhlar, D. G. *J. Am. Chem. Soc.* **1990**, *112*, 3347.

(22) Ohta, K.; Morokuma. K. *J. Phys. Chem.* **1985**, *89*, 5845.

(23) Morokuma, K. *J. Am. Chem. Soc.* **1982**, *104*, 3732.

(24) Tachikawa, H. *J. Phys. Chem. A* **2000**, *104*, 497.

(25) (a) Tachikawa, H. *Phys. Chem. Chem. Phys*. **1999**, *1*, 2675. (b) Tachikawa, H. *Phys. Chem. Chem. Phys.* **1999**, *1*, 4925. (c) Tachikawa, H. *J. Phys. Chem. A* **1998**, *102*, 7065. (d) Tachikawa, H.; Igarashi, M. *J. Phys. Chem. A* **1998**, *102*, 8648. (e) Tachikawa, H. *J. Phys. Chem. A* **1997**, *101*, 7475. (f) Tachikawa, H. *J. Phys. Chem. A* **1999**, *103*, 6873. (g) Tachikawa, H. *Phys. Chem. Chem. Phys.* **2000**, *2*, 839. (h) Program code of the direct ab initio dynamics calculation was created by our group.

(26) Ab initio MO calculation program: Frisch, M. J.; Trucks, G. W.; Schlegel, H. B.; Gill, P. M. W.; Johnson, B. G.; Robb, M. A.; Cheeseman; J. R.; Keith, T.; Petersson, G. A.; Montgomery, J. A.; Raghavachari, K.; Al-Laham, M. A.; Zakrzewski, V. G.; Ortiz, J. V.; Foresman, J. B.; Cioslowski, J.; Stefanov, B. B.; Nanayakkara, A.; Challacombe, M.; Peng, C. Y.; Ayala, P. Y.; Chen, W.; Wong, M. W.; Andres, J. L.; Replogle, E. S.; Gomperts, R.; Martin, R. L.; Fox, D. J.; Binkley, J. S.; Defrees, D. J.; Baker, J.; Stewart, J. P.; Head-Gordon, M.; Gonzalez, C.; Pople, J. A. *Gaussian 94*, Revision D.3; Gaussian, Inc.: Pittsburgh, PA, 1995.